International Journal of Nanomedicine

Dovepress
open access to scientific and medical research

Open Access Full Text Article

ORIGINAL RESEARCH

A Novel Targeted Therapy System for Cervical Cancer: Co-Delivery System of Antisense LncRNA of MDC1 and Oxaliplatin Magnetic Thermosensitive Cationic Liposome Drug Carrier

This article was published in the following Dove Press journal:
International Journal of Nanomedicine

Hui Ye[1,*]
Xiaoying Chu[1,*]
Zhensheng Cao[2,*]
Xuanxuan Hu[1,*]
Zihan Wang[2]
Meiqi Li[1]
Leyu Wan[2]
Yongping Li[3]
Yongge Cao[4]
Zhanqiu Diao[2]
Fengting Peng[2]
Jinsong Liu[2]
Lihua Xu[5]

[1]School of Basic Medical Sciences, Wenzhou Medical University, Wenzhou, Zhejiang, 325035, People's Republic of China; [2]School of Stomatology, Wenzhou Medical University, Wenzhou, Zhejiang, 325035, People's Republic of China; [3]Department of Surgery, Chengdu Shuangliu District Maternal and Child Health Hospital, ChengDu, Sichuan, 610200, People's Republic of China; [4]Department of Stomatology, Haiyuan College, Kunming, Yunnan, 650106, People's Republic of China; [5]Department of General Medicine, First Affiliated Hospital, Wenzhou Medical University, Wenzhou, 325000, People's Republic of China

*These authors contributed equally to this work

Correspondence: Hui Ye
School of Basic Medical Sciences, Wenzhou Medical University, Wenzhou, Zhejiang, 325035, People's Republic of China
Email wmcyh@wmu.edu.cn

Lihua Xu
Department of General Medicine, First Affiliated Hospital, Wenzhou Medical University, Wenzhou, 325000, China
Email lihuaxu@wmu.edu.cn

Background: This study was aimed to prepare a novel magnetic thermosensitive cationic liposome drug carrier for the codelivery of Oxaliplatin (OXA) and antisense lncRNA of MDC1 (MDC1-AS) to Cervical cancer cells and evaluate the efficiency of this drug carrier and its antitumor effects on Cervical cancer.

Methods: Thermosensitive magnetic cationic liposomes were prepared using thin-film hydration method. The OXA and MDC1-AS vectors were loaded into the codelivery system, and the in vitro OXA thermosensitive release activity, efficiency of MDC1-AS regulating MDC1, in vitro cytotoxicity, and in vivo antitumor activity were determined.

Results: The codelivery system had desirable targeted delivery efficacy, OXA thermosensitive release, and MDC1-AS regulating MDC1. Codelivery of OXA and MDC1-AS enhanced the inhibition of cervical cancer cell growth in vitro and in vivo, compared with single drug delivery.

Conclusion: The novel codelivery of OXA and MDC1-AS magnetic thermosensitive cationic liposome drug carrier can be applied in the combined chemotherapy and gene therapy for cervical cancer.

Keywords: magnetic thermosensitive cationic liposome, oxaliplatin, antisense lncRNA of MDC1, targeted therapy, cervical cancer

Introduction

Cervical cancer is one of the most common malignant tumors in women. The incidence and mortality of Cervical cancer in women rank second in developing countries. The incidence of Cervical cancer increases by 2–3% annually. Thus, this disease severely threatens women's health.[1,2] After surgery, distant metastasis has been observed in some patients, and tumor recurrence often occurs in some patients. Chemotherapy has become an important means to treat cervical cancer.[3,4] However, traditional chemotherapy exerts poor therapeutic effect and side effects in clinical applications. For example, oxaliplatin (OXA) exhibits broad-spectrum in vitro cytotoxicity and in vivo antitumor activity in multiple tumor model systems. Nevertheless, this drug causes neurotoxicity, gastrointestinal abnormal reaction, hemorrhage, allergic reaction, and severe adverse reactions.[5,6] Overall, traditional chemotherapy requires systemic administration, has no targeting property and controlled release, and cannot deliver effective drug concentrations to the tumor, resulting in numerous adverse effects.[7]

Therefore, multiagent codelivery systems have been established. The combination of dendrosomal nano curcumin and OXA has displayed a distinguished cell death effect on human ovarian carcinoma cell lines.[8] In addition, enhanced antitumor activity has also been demonstrated by combined OXA and ginsenoside Rg3 in hepatocellular carcinoma cells.[9] This approach can deliver simultaneously two different types of drugs to the same tumor cells and exert a synergistic antitumor effect.[10,11] For example, two chemotherapeutic drugs with different mechanisms are delivered or a type of chemotherapeutic drug is combined with long noncoding RNA (LncRNA) for a certain oncogene or antioncogene. Combined gene therapy exhibits a synergistic antitumor effect with chemotherapy. Targeted delivery and drug-controlled release can improve the antitumor effect and reduce the side effects of chemotherapy drugs.[7]

Studies have demonstrated that an important category of lncRNAs was transcripts from the opposite strand to a protein coding gene, called antisense lncRNAs.[12,13] Several cancer-related genes, such as ADAMTS9 and Myc, have already been demonstrated to be regulated by their antisense lncRNAs.[14,15] One of the regulatory mechanisms of antisense lncRNAs is that they can form RNA–RNA dimer with the mRNA of neighboring genes and thereby protect the mRNA from being degraded by RNase. This process increases the stability of the mRNA and elevates the expression level of the coding gene.[16] In 2015, Xue et al found that the expression levels of the Mediator of DNA damage Checkpoint 1 (MDC1) and its antisense lncRNA (MDC1-AS) were downregulated in bladder cancer.[17] After the overexpression of MDC1-AS, increased levels of MDC1 were observed in the bladder cancer cells. In 2016, Yue et al showed that the expression levels of MDC1-AS and MDC1 were significantly downregulated in glioma tissues compared with normal brain tissues, and MDC1-AS expression was positively correlated with MDC1 expression.[18] These observations were consistent with previous studies that reported a decreased MDC1 level in cancerous tissues.[19,20] Hence, MDC1-AS is a potential therapeutic target for the treatment of Cervical cancer.

Liposomes (LPs) are excellent chemotherapy drugs or nucleic acid (ie, DNA and RNA) carriers. Numerous delivery platforms, such as LPs, micelles, layer-by-layer assembly technology, microencapsulation, and stimulus-sensitive polymers, have been applied in cancer therapy. Among these platforms, the LP exhibits high stability, hypotoxicity, and the multifunction potential after proper modification.[21] LPs can be divided into various types according to their diverse characteristics. As a new type of targeted drug delivery system, magnetic thermosensitive liposomes (MTLs) are prepared by adding magnetic substances, such as Fe_2O_3 or Fe_3O_4, and therapeutic drugs in thermo-sensitive LPs.[22,23] Magnetic nanoparticles are used as heating elements to control drug release by alternating magnetic field (AMF) in vitro. These particles are also employed to reach the phase transition temperature of LPs and achieve targeted, multiple, and pulse-type drug delivery in tumor tissues, overcoming certain adverse reactions. This approach improves the compliance and quality of life of patients undergoing cancer chemotherapy, presenting potential for clinical applications. A lipoplex (LP-nucleic acid complex) forms when the positive charge of an LP interacts with the negative charge of DNA or RNA. This type of LP, which possesses low toxicity and immunogenicity, is an effective gene delivery vector.[24] Various cationic LPs have been used in genetic engineering experiments.[25] Therefore, cationic liposomes CLs can be applied to transfect plasmid encoding lncRNAs into tumor cells for gene therapy for cancer cells.

The authors speculate that the combination of gene therapy and chemotherapy could significantly improve the outcomes of treatment for Cervical cancer. Therefore, this study was performed to integrate the characteristics of magnetic LP (ML), thermosensitive LP (TL), and CL to design a codelivery carrier of chemotherapeutic drugs and plasmid encoding LncRNAs with magnetic targeting capability and thermal controlled release. The proposed approach can not only deliver simultaneously chemotherapeutic drugs and plasmid-encoding LncRNAs but also achieve local magnetic targeted delivery to the tumor and temperature-induced drug release under the effects of in vitro directed magnetic field and AMF. The treatment effects were assessed based on the OXA thermosensitive release, ability of MDC1-AS to regulate MDC1, and magnetic targeted delivery of OXA and MDC1-AS. In vitro cytotoxicity and apoptosis induction test, in vivo tumor inhibition test, quantitative real-time PCR, and Western blot analysis were also performed.

Materials and Methods

Chemicals and Reagents

1.2-Dipalmitoyl-sn-glycero-3-phosphocholine (DPPC), and 3 ß -[N- (N', N' - dimethylaminoethane)- carbamoyl]cholesterol (DC-Chol) were purchased from Avanti Polar Lipids (USA). Cholesterol, Dimethyldioctadecyl ammonium

bromide (DOAB), Triton X-100 and oxaliplatin were obtained from Sigma-Aldrich (Saint Louis, USA). Sephadex G-50 was purchased from Pharmacia Fine Chemicals (Uppsala, Sweden). Ultrafine magnetite (Fe_3O_4, mean diameter 10 nm) was received from the Southwest Institute of Applied Magnetics of China (Chengdu, China). pcDNA 3.1 vector and pcDNA 3.1-EGFP vector were provided by Invitrogen (Carlsbad, USA). Cell Count Kit-8 was received from Dojindo (Kyushu, Japan). AnnexinV–FITC/Propidium iodide apoptosis detection kit was supplied by Abcam (Cambridge, UK). Lipofectamine 2000 reagent, Trizol reagent, deoxyribonuclease I enzyme, SuperScript® III Reverse Transcriptase, PCR Master Mix, and SYBR Green PCR Master Mix were purchased from Invitrogen (Carlsbad, USA). BCA protein assay kits were acquired from Pierce (Rockford, USA). Polyvinylidene difluoride membranes were acquired from Bio-Rad Laboratories (Hercules, USA). Antibodies of rabbit anti-human MDC1, Bcl-2, and Bax were purchased from Abcam (Cambridge, UK). Horseradish peroxidase-conjugated goat antirabbit IgG and electrochemiluminescence kits were supplied from Amersham Pharmacia Biotech (Piscataway, USA). All other chemicals were of commercial analytical grade.

Cells and Animals

SiHa cell line (RRID: CVCL_0032) was purchased from Cell Bank of Type Culture Collection of the Chinese Academy of Sciences in Shanghai, China. All human cell lines have been authenticated using STR profiling within the last three years and that all experiments were performed with mycoplasma-free cells. The cells were cultured in alphaMEM medium (Invitrogen, USA) supplemented with 10% Fetal bovine serum (FBS) (Sigma, USA), 100 U/mL penicillin, and 50 μg/mL streptomycin (Mediatech, USA) and incubated at 37°C with 5% CO_2, and trypsin were supplied from Invitrogen (Carlsbad, CA, USA).

Six-week-old athymic BALB/Ca nu/nu female mice (18–20 g) were purchased from the Shanghai Laboratory Animal Center of Chinese Academy of Sciences (Shanghai, China). BALB/Ca nu/nu mice were housed at constant room temperature under specific pathogen-free conditions and provided with a 12 h: 12 h light/dark cycle, standard rodent diet, and water ad libitum. All animal experiments were approved and evaluated by the Animal and Ethics Review Committee of Wenzhou Medical University (Wenzhou Medical University Policy and Welfare Committee followed by Laboratory animal-Guideline for ethical review of animal welfare, GB/T 35892–2018 of CHINA, Document ID: WMU-2011- AP-0013).

Preparation of MTCL-OXA-MDC1-AS

The total RNA was isolated from the SiHa cells by using Trizol reagent. The complementary DNA (cDNA) was synthesized with total RNA by using SuperScript® III Reverse Transcriptase. Then, the full length of the cDNA encoding MDC1-AS was amplified by PCR, *GAPDH* gene was used as an internal control, Primers were designed as previously described and are listed in Table 1.[18] The vectors expressing MDC1-AS were prepared by cloning the amplified fragments into the pcDNA 3.1 or pcDNA 3.1-EGFP vector. Plasmid reconstruction is illustrated in Figure 1A.

According to the weight ratio of DPPC:DC-Cholesterol :DOAB:cholesterol (17.08:0.81:0.90:1.21), 20 mg of total phospholipid was placed in a round-bottomed flask. The solution was added with 10 mL of chloroform–methanol solution (2:1, volume ratio). Decompression evaporation was performed at 37°C for 1 h to form a layer of phospholipid film on the bottom of the flask. The solution was then added with 1 mL of Fe_3O_4 and ammonium sulfate suspension membrane. Extrusion of polycarbonate filter and ammonium sulfate gradient method were used to

Table 1 Sequences of Primers Used in RT-PCR Assay

Gene	Sense (5′-3′)	Antisense (5′-3′)
MDC1-AS	TCCCAGATGTGCCAAAGTCAG	AGCAACCCCAGTTGTCATTC
MDC1	GCAGCTTCCAGACAACAG	TACCCATGACTTTATCCACA
Bcl-2	TTGGATCAGGGAGTTGGAAG	TGTCCCTACCAACCAGAAGG
BAX	AGGATGCGTCCACCAAGAAG	GAGTCTCACCCAACCACCCT
GAPDH	GCCAAAAGGGTCATCATCTC	GCCTTCAACGCCTGCTTC

Notes: Primer sequences of genes used in the study are provided as above.

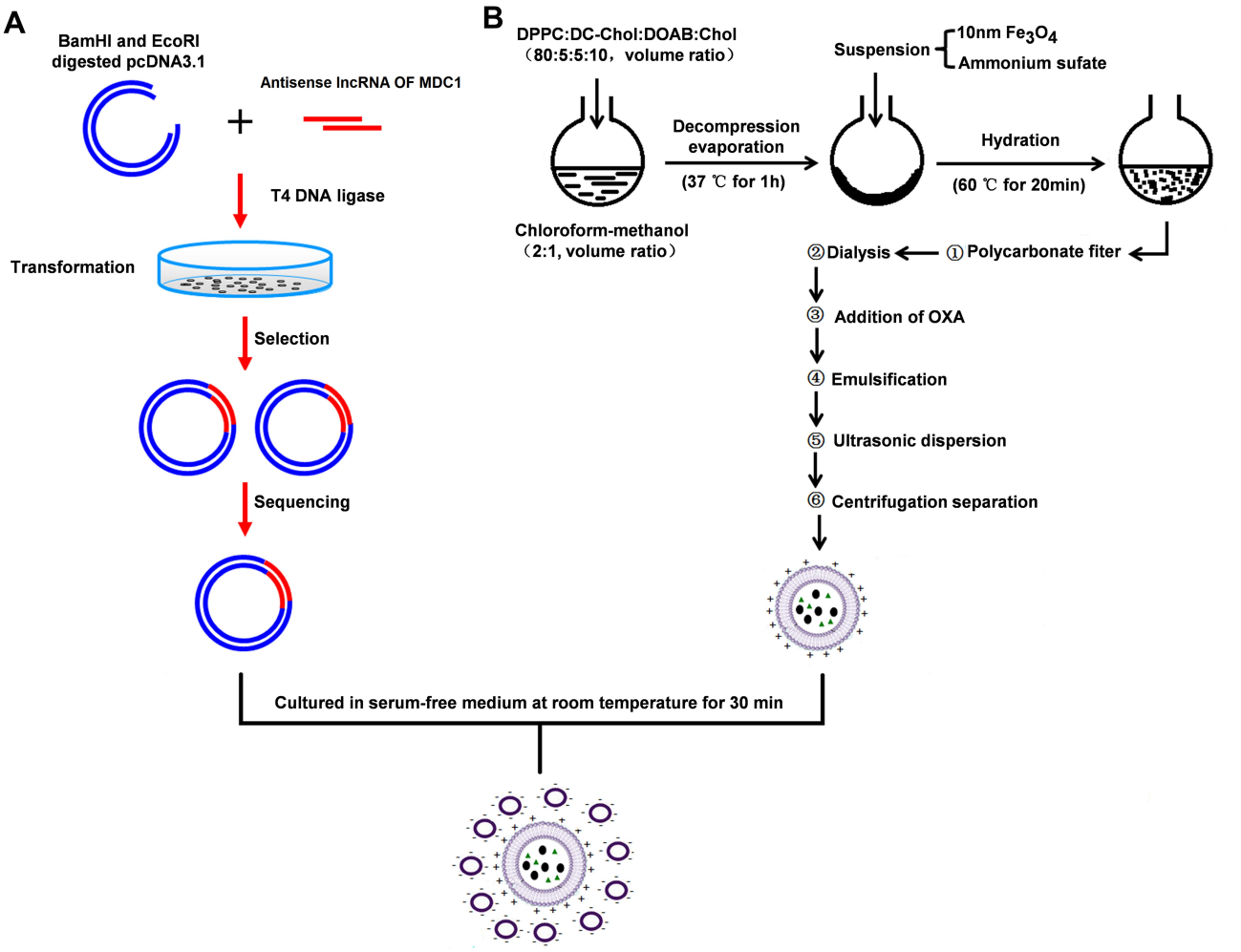

Figure 1 Preparation flow of MTCL–OXA–MDC1-AS. (**A**) Sketch map of pcDNA-MDC1-AS: Total RNA was isolated from SiHa cells, and cDNA synthesis was performed with total RNA. Then, complementary DNA encoding MDC1-AS was amplified by PCR. The vectors expressing MDC1-AS were prepared by cloning the amplified fragments into pcDNA 3.1 vector or pcDNA 3.1-EGFP vector; (**B**) Preparation flow of MTCL–OXA–MDC1-AS: According to weight ratio of DPPC: DC-Cholesterol: DOAB: Cholesterol = 17.08:0.81:0.90:1.21, 20 mg of total phospholipid was placed in a round-bottom flask. The solution was added with 10 mL of chloroform–methanol solution. Decompression evaporation was performed at 37 °C for 1 h to form a layer of phospholipid film on the bottom of the flask. The solution was then added with 1 mL of Fe_3O_4 and ammonium sulfate suspension membrane. Extrusion of polycarbonate filter and ammonium sulfate gradient method were used to seal OXA into LP. The mixture was centrifuged to remove the unsealed Fe_3O_4 and form MTCL–OXA. Finally, the pcDNA–MDC1-AS plasmid and MTCL–OXA were cultured in serum-free medium at room temperature for 30 min to prepare MTCL–OXA–MDC1-AS.

seal OXA into the LP. The solution was centrifuged (1000×g, 15 min) to remove the unsealed Fe_3O_4 and form magnetic thermosensitive cationic liposome drug carrier, carrying OXA (MTCL-OXA). Finally, the pcDNA-MDC1-AS plasmid and MTCL-OXA were cultured in a serum-free medium at room temperature for 30 min to prepare MTCL-OXA-MDC1-AS (Figure 1B). In the above preparation process, TCL-OXA (thermosensitive cationic liposome as the carrier to deliver OXA), TCL-MDC1-AS (thermosensitive cationic liposome as the carrier to deliver MDC1-AS), and MTCL-OXA-MDC1-AS (MTCL as the carrier to codeliver OXA and MDC1-AS) were prepared without a magnetic flow field.

Morphological and Biophysical Characteristics

Appropriate amounts of MTCL-OXA-MDC1-AS were diluted with distilled water. The mixture was dropped on a special copper mesh and left undisturbed for 1 min. Then, 3% phosphotungstic acid was used for negative staining. The net was left to stand for 20 s to allow the deposition of particles onto the net. The size and morphology of the particle were assessed through transmission electron microscopy (TEM) (the size and morphology of TCL-OXA and TCL-MDC1-AS can be observed without the copper net). The diluted LP suspension was poured into a cuvette, which was placed in a laser particle size

analyzer at 25°C. Dynamic light scattering theory was used to detect the particle size and scattering property of the LP. Electrophoretic mobility was assessed to determine the surface potential. Quantitative and encapsulation efficiency in TCL-OXA, TCL-MDC1-AS, and MTCL-MDC1-AS (magnetic thermosensitive cationic liposome drug carrier, carrying the antisense lncRNA of MDC1) in OXA was determined using the method proposed by Ye.[26]

Determination of Thermosensitive Release Rate of the OXA Liposome

The release behavior of drugs from the OXA LP suspension at 37°C and 42°C was studied by the dialysis method. The dialysis tube (14,000 MWCO) containing 1 mL of the OXA LP suspension was transferred to a beaker containing 50 mL of phosphate-buffered saline (PBS) by maintaining the temperature at 37°C and 42°C with continuous stirring at 100 rpm. The sink condition was maintained by periodically removing 1 mL of the sample and replacing an equal volume of PBS at 0, 5, 10, 15, 30, 60, and 90 min. The amount of OXA released was analyzed with HPLC.

Determination of Transfection Efficiency

The SiHa cells were cultured in alpha MEM medium containing 10% FBS in an incubator under 5% CO_2 at 37°C. The SiHa cells were inoculated in a 12-hole cell culture plate overnight until 90% fusion one day before transfection. The mock group (the complex of pcDNA3.1-EGFP empty vector and Lipofectamine 3000), TCL-MDC1-AS group, and MTCL-MDC1-AS group were added into the 12-well plate, respectively. Then, 5000GS external magnetic field was applied to the bottom of the 12-well plate for 30 min. After transfection for 6 h, the culture medium was changed into alpha MEM complete medium containing 10% FBS. The medium was then placed in an incubator and cultured for 48 h. A fluorescence microscope was used to determine the expression level of EGFP in the SiHa cells and evaluate the transfection efficiency. Other details have been reported in other studies.[27]

Effect of MTCL-MDC1-as on Cell Proliferation

The cells in the logarithmic growth phase were obtained for inoculation in a 96-hole plate. The SiHa cells were randomly divided into three groups, namely, mock (the complex of pcDNA3.1 empty vector and Lipofectamine 3000), TCL-MDC1-AS, and MTCL-OXA-MDC1-AS groups, with five small holes for each group. After the corresponding reagents were added into all groups, 5000GS external magnetic field was applied to the bottom of the 96-hole culture plate, and the temperature was increased to 42°C and maintained for 30 min. After transfection for 6 h, 100 μL of the culture medium containing 10% FBS was placed in each hole for continuous culture. The culture medium was replaced with a medium containing 10% CCK-8 to attain a continuous culture for 2 h after interfering for 24, 48, and 72 h. Then, the absorbance at 450 nm was determined using a microplate reader.

Cell inhibition rate= [1−(experiment group A value/mock group A value)] × 100

Effect of MTCL-MDC1-AS on Cell Apoptosis

The groups were divided using the methods in previous sections. After digestion, the SiHa cells were inoculated in 12-hole culture plates and added with the corresponding reagents. A 5000GS external magnetic field was applied to the bottom of the 12-hole culture plate. The temperature was increased to 42°C and maintained for 30 min. Digestion occurred after the cells were cultured in the cell medium for 48 h. Three groups of 2×10^5 cells were placed in 500 μL of the combined buffer liquid after washing twice with PBS. AnnexinV–FITC (5 μL) and propidium iodide dye liquor (5 μL) were added in the dark for 30 min at room temperature. Flow cytometry was used to determine the apoptosis rate in each group. Details of the experiment have been reported.[5]

Transwell Cell Migration and Invasion Assay

The SiHa cells were seeded in 12-well plates, and the groups were divided into six groups, namely, the control (without treatment), OXA, TCL-OXA, TCL-MDC1-AS, TCL-OXA-MDC1-AS, and MTCL-OXA-MDC1-AS groups. The OXA dosage was 20 μg/mL, while that of pcDNA–MDC1-AS was 1.5 μg/hole. A 5000GS external magnetic field was applied to the bottom of the 12-hole culture plate. The temperature was increased to 42°C and maintained for 30 min. After 48 h of incubation, the culture medium containing 1% serum of each group was used to resuspend the cells. In brief, 5×10^4 cells were added into the upper chamber of each Transwell membrane, and 600 μL of the culture liquid containing 10%

FBS was added into the lower chamber. The system was then placed in 5% CO_2 at 37°C. After culturing for 24 h in a saturated humid environment, the culture liquid in the upper chamber was discarded. Then, 4% paraformaldehyde was added for fixing for 15 min at room temperature after two to three times of PBS washing. A cotton swab was used to absorb the liquid inside the upper chamber. A 1% Crystal Violet staining solution was used to dye for 15 min at room temperature. After two to three times of PBS washing, five vision fields were considered for each hole at random to take photos under a microscope. The number of cells was counted and averaged.

Precooled Matrigel glue and alpha MEM medium without serum were diluted at a proportion of 1:8 to coat the transwell membrane between the upper and lower chambers. The chamber was placed in an incubator for 30 min to produce a glue. The other steps were identical to those of the migration experiment.

Establishment of the Animal Model and in vivo Tumor Inhibition Test

Balb/c nude mice were fed in a laminar animal house, which was especially made for Laboratory Animal Center, Wenzhou Medical University. The SiHa cells in the logarithmic growth phase were harvested to prepare a single-cell suspension. Then, 200 μL of the suspension volume was injected into the subcutaneous part of the flank of the nude mice. As shown in Figure 2A, after 2 weeks, the nude mice with transplanted tumor of approximately 0.8 cm diameter and good growth performance were selected as animal models.

Thirty-six tumor-bearing mice were randomly divided into six groups (n=6) and injected with normal saline (Control), OXA, TCL-OXA, TCL-MDC1-AS, TCL-OXA-MDC1-AS, and MTCL-OXA-MDC1-AS through the caudal vein. The OXA dosage was 5 μg of OXA/g (body weight), and pcDNA–MDC1-AS dose was 8 μg for each mouse. One injection was conducted every 3 days (Figure 2B). After each injection, a 5000GS directed magnetic field was applied to the tumor site on the body surface for 30 min to achieve the magnetic targeting of drugs. Under the effect of the AMF (H=12 KA/m, f=250 kHz), complete cytoreduction was locally heated to 42°C to achieve the thermosensitive release of drugs. Three therapy cycles were conducted. After therapy, the transplanted tumor was measured once every 2 days (the maximum diameter of tumor a and short diameter were perpendicular to the maximum diameter b and tumor volume, that is, $V=ab^2/2$). After treatment, the animals were killed on the 30th day. Transplanted tumors were removed from the subcutaneous parts of all animals. The tumors were weighed and stored in liquid nitrogen, and the tumor inhibition rate was calculated according to the literature.[7] The same method was used to establish another 36 nude mouse models of cervical cancer transplantation, in which the grouping and administration were the same as mentioned above, and the survival of the nude mice was recorded.

Detection of Apoptosis-Related Genes in the Cervical Cancer Through RT-QPCR Analyses

Trizol reagent was used to extract the total RNA of tumor tissues. SuperScript®III Reverse Transcriptase was applied for the reverse transcription to form cDNA. Real-time Fluorescent Quantitative PCR was conducted using SYBR Green PCR Master Mix, which was purchased from Invitrogen (Carlsbad, USA) and used according to the manufacturer's instruction. Each gene primer sequence is listed in Table 1. The test was repeated thrice. Changes in the mRNA relative internal control contents of all groups were compared (target gene gray/internal control gray).

Detection of Apoptosis-Related Genes in the Cervical Cancer Through Western Blot Analysis

The protein from the tumor tissue was extracted to measure the protein content by using BCA method. The loading buffer was added to perform SDS-PAGE. The protein content in each hole was approximately 50 μg. Immunoblot was performed using primary antibodies against Rabbit anti-human MDC1, BCL-2, and BAX antibodies and HRP–conjugated secondary antibodies. Enhanced chemiluminescence method was used to observe and analyze changes in the color of the strips. β-actin was used as reference. Densitometry analysis of the band value of the strips was performed.

Statistical Method

Data were statistically processed using SPSS11.5 software package. Groups were compared through homogeneity test of variance and factor analysis of variance (one-way ANOVA). If $P<0.05$, then the difference was considered significant.

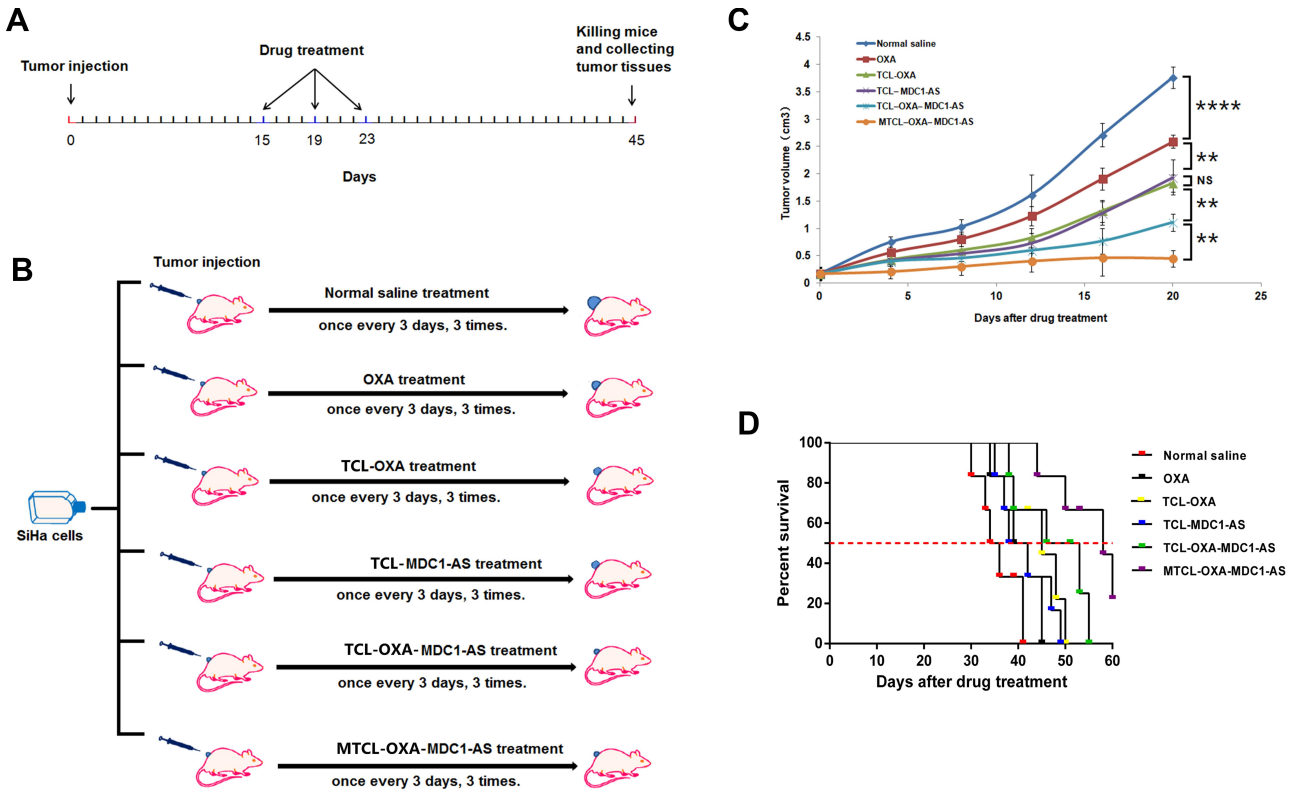

Figure 2 Sketch map of the drug administration in nude mice with cervical cancer and the in vivo anti-tumor test result. (**A**) The drug administration of nude mice with cervical cancer: the nude mice with cervical cancer were injected with normal saline, OXA, TCL-OXA, TCL-MDC1-AS, TCL-OXA-MDC1-AS, and MTCL-OXA-MDC1-AS on the tail vein once every 3 days. After each injection, 30 min 5000GS directed magnetic field was applied on the surface of the tumor site to achieve magnetic targeting of drugs. Then, under the effect of AMF (H=12 KA/m, f=250 kHz), the local temperature of the tumor site was increased to 42 °C to achieve the thermosensitive release of drugs. Treatment was introduced three times. (**B**) Sketch map of the drug administration strategy for nude mice with Cervical cancer. (**C**, **D**) In vivo anti-tumor test (C: Size of transplanted tumor, (**D**) Survival curve). **P<0.01, ****P<0.0001.

Results

Preparation and Characterization of MTCL-OXA-MDC1-AS

The pcDNA-MDC1-AS expression vector was prepared by amplifying the full length of cDNA encoding MDC1-AS, and the amplified fragments were then cloned into the pcDNA 3.1 vector. The amplified fragments were then sequenced to confirm no errors in the nucleotides. This finding indicated the successful construction of the pcDNA-MDC1-AS expression vector for the MDC1-AS gene target sequence.

The TEM image showed that the MTCL exhibited a spherical structure. Fe_3O_4 particles were enclosed in the LP membrane, indicating stronger staining. As shown in Table 2, the particle diameter of TCL was 86.5± 9.3 nm. The particle diameter of TCL-OXA increased to 138.3±8.1 nm because of the enclosed OXA (P<0.05). Moreover, the particle diameters of TCL-MDC1-AS and MTCL-OXA-MDC1-AS significantly increased because of the pcDNA absorption (P<0.05). For ML, the particle diameters of MTCL, MTCL-OXA, TCL-MDC1-AS, and MTCL-OXA-MDC1-AS were 140.6±15.9, 178.3±16.1, 243.0±13.4, and 350.5±21.7 nm (Figures S1A and S1B), respectively, which were significantly higher than those of TCL, TCL-OXA, TCL-MDC1-AS, and MTCL-OXA-MDC1-AS (P<0.05). The encapsulation efficiencies of TCL-OXA and MTCL-OXA were 88.7%±7% and 78.2%±4%, respectively (n=3). The encapsulation efficiencies of TCL-OXA-MDC1-AS and MTCL-OXA-MDC1-AS were 83.4% ±3% and 70.1%±6%, respectively (n=3). Hence, the absorption of the MDC1-AS plasmid did not induce the leakage of OXA in the LP.

Determination of OXA Thermosensitive Release Rate

As shown in Figures S2A and S2B, when the temperature reached 37°C, the OXA release rates of TCL-OXA and MTCL-OXA in PBS at 60 min were 19% and 18%, respectively, and those of TCL-OXA-MDC1-AS and MTCL-OXA-MDC1-AS in PBS at 60 min were 14% and 16%, respectively (Figures S2C and S2D). These results show that TCL-OXA, MTCL-OXA, MTCL-OXA-

Table 2 Particle Size, Polydispersion, and Zeta Potential of Liposomes (n=3)

Groups	Particle Size (nm)	Polydispersion	Zeta Potential (mV)
TCL	86.5±9.3	0.183±0.032	+59.3±6.2
TCL-OXA	138.3±8.1	0.227±0.025	+56.0±4.1
TCL-MDC1-AS	176.2±12.5*	0.205±0.019	+41.4±5.9*
TCL-OXA-MDC1-AS	262.7±17.3*	0.301±0.051	+30.2±5.0*
MTCL	140.6±15.9#	0.246±0.034	+50.5±6.4
MTCL-OXA	178.3±16.1#	0.238±0.028	+53.2±3.7
MTCL-MDC1-AS	243.0±13.4*,#	0.262±0.021	+29.8±5.4*
MTCL-OXA-MDC1-AS	350.5±21.7*,#	0.299±0.046	+21.5±4.3*

Notes: *P<0.05, TCL–MDC1-AS vs TCL; TCL–OXA–MDC1-AS vs TCL–OXA; MTCL–MDC1-AS vs MTCL; MTCL–OXA–MDC1-AS vs MTCL–OXA. #P<0.05, MTCL vs TCL; MTCL–OXA vs TCL–OXA; MTCL–MDC1-AS vs TCL–MDC1-AS, and MTCL–OXA–MDC1-AS vs TCL–OXA–MDC1-AS.

MDC1–AS, and MTCL-OXA-MDC1–AS were unchanged at 37°C. Furthermore, the absorption of plasmid DNA did not significantly affect stability (P >0.05).

When the temperature reached 42°C, the OXA release rates of TCL-OXA and MTCL-OXA in PBS at 60 min increased to 42% and 44%, respectively. The OXA release rates of TCL-OXA-MDC1-AS and MTCL-OXA-MDC1-AS in PBS at 60 min were 39% and 40%, respectively. The OXA release rates of TCL-OXA, MTCL-OXA, TCL-OXA-MDC1-AS, and MTCL-OXA-MDC1-AS at 42°C were significantly higher than those at 37°C. These results showed that LP based on TCL exhibited efficient OXA thermosensitive release and could be used to induce OXA thermosensitive-controlled release triggered by AMF in vitro.

Effect of MTCL-MDC1-AS on Cell Proliferation and Apoptosis

The transfection efficiency of the MDC1-AS gene in the Cervical cancer cells was also evaluated using TCL-MDC1-AS and MTCL-MDC1-AS. As shown in Figure 3 A1-3 and B1-3, compared with TCL-MDC1-AS, the combined effect of MTCL-MDC1-AS and in vitro directed magnetic field could significantly improve the gene transfection efficiency (P<0.01). This result suggested that application of magnetic LP and in vitro directed magnetic field could help MDC1-AS gene play a better role in tumor inhibition.

The proliferation of the SiHa cells in all groups at any time point is shown in Table 3. MDC1-AS significantly inhibited SiHa cell proliferation. After transfection for 24, 48, and 72 h, the inhibition rates in the TCL-MDC1-AS group were 4.3% ± 1.5%, 16.9% ± 3.5%, and 30.9% ± 4.3%, respectively. The corresponding inhibition rates in the MTCL-MDC1-AS group were 13.7% ± 1.9%, 30.0% ± 7.2%, and 44.5% ± 4.3%. The inhibition rates of MTCL-MDC1-AS were significantly higher than those of the TCL-MDC1-AS (P<0.01) and mock (P<0.0001) groups, and the highest inhibition rates were observed after 72 h (Figure 3C).

As shown in Figure 3 D1-3, based on the flow cytometry results, the apoptotic rates of SiHa cells in the control and experiment groups were 3.6% ± 1.5% (mock group), 18.9% ± 2.6% (TCL-OXA-MDC1-AS group), and 29.9% ± 2.5% (MTCL-OXA-MDC1-AS group). The apoptotic rates of MTCL-MDC1-AS were significantly higher than those of TCL-MDC1-AS (P<0.01) and mock (P<0.001) groups (Figure 3D).

Transwell Small-Chamber Migration and Invasion Test

After the OXA thermosensitive release rate and effect of MTCL-MDC1-AS on cell proliferation and apoptosis were determined, whether MTCL-OXA-MDC1-AS participated in cell migration and invasion was investigated. As shown in Figure 4 A1-6 and C, the numbers of SiHa cells that migrated in the control and experiment groups were 792 ± 46 (Control group), 616 ± 23 (OXA group), 409 ± 27 (TCL-OXA group), 390 ± 16 (TCL-MDC1-AS group), 225 ± 41 (TCL-OXA-MDC1-AS group), and 151 ± 24 (MTCL-OXA-MDC1-AS group). Then, in the evaluation of cell invasion, Figures 4 B1-6 and Figure 4D showed that the invasion number of the SiHa cells in the control and experiment groups were 576 ± 23 (Control group), 433 ± 29 (OXA group), 313 ± 26 (TCL-OXA group), 286 ± 11 (TCL-MDC1-AS group), 182 ± 9 (TCL-OXA-MDC1–AS group), and 108 ± 25 (MTCL-OXA-MDC1–AS group). These results indicated that MTCL-OXA-MDC1–AS could significantly inhibit the migration and invasion activity of the SiHa cells.

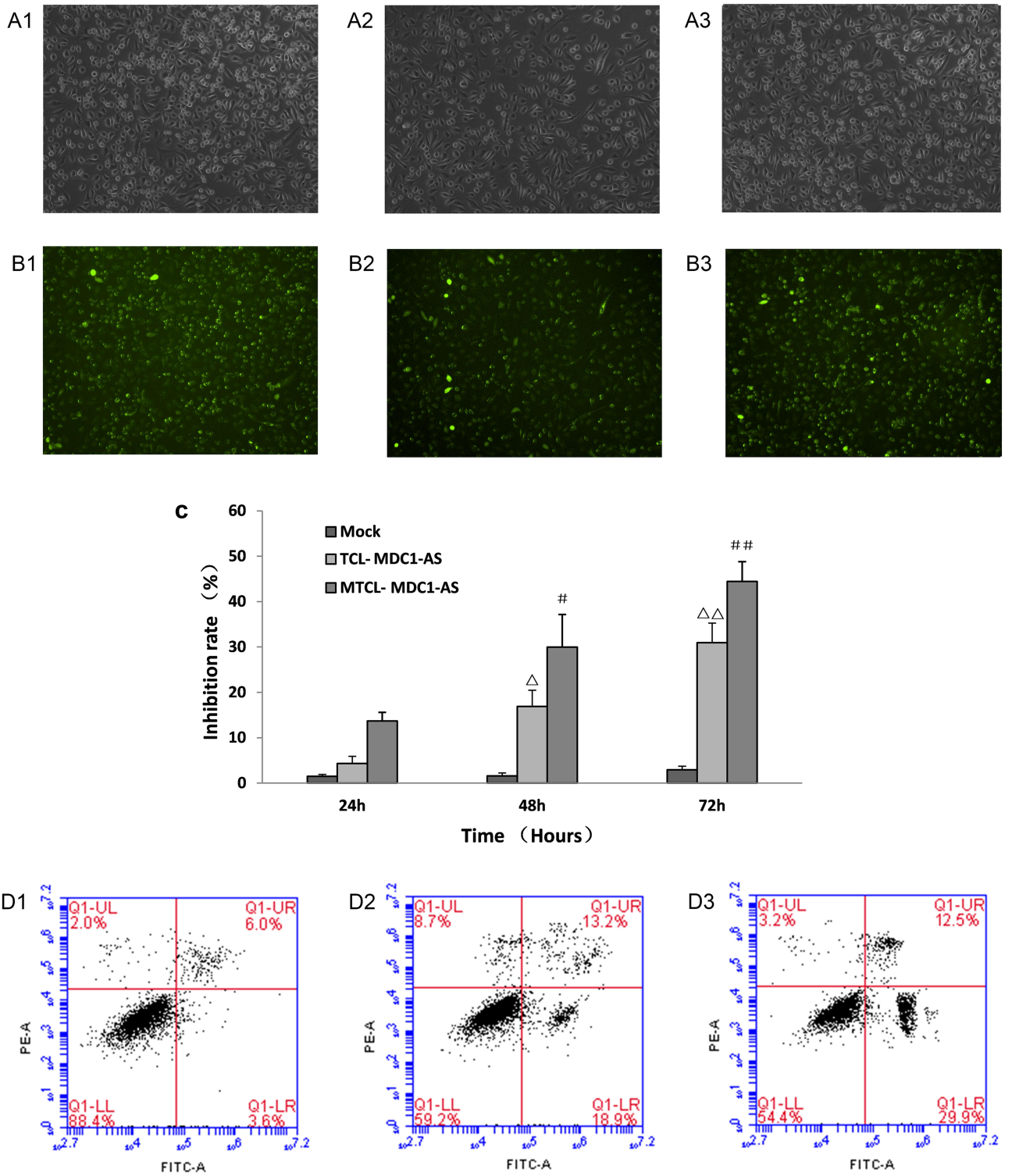

Figure 3 Effect of MTCL–MDC1-AS on SiHa cells. (**A**) Morphology of SiHa cells in each group before transfection: A1, A2, and A3 represent the morphology of SiHa cells before transfection with mock, TCL–MDC1-AS, and MTCL–MDC1-AS, respectively; (**B**) Fluorescence imaging of SiHa cells in each group after transfection: B1, B2, and B3 represent the fluorescence imaging of SiHa cells transfected by using mock, TCL–MDC1-AS, and MTCL–MDC1-AS, respectively; (**C**) The changes in cell proliferation in SiHa cells transfected using TCL–MDC1-AS and MTCL–MDC1-AS: the values are expressed as mean ± SD from three independent experiments. $^{\Delta}P<0.01$ compared with 24 h of TCL–MDC1-AS; $^{\Delta\Delta}P<0.0001$ compared with 24 h of TCL–MDC1-AS; $^{\#}P<0.001$ compared with 24 h of MTCL–MDC1-AS; $^{\#\#}P<0.0001$ compared with 24 h of MTCL–MDC1-AS–AS. (**D**) Comparison of the apoptosis rates of SiHa cells transfected using TCL–MDC1-AS and MTCL–MDC1-AS: The apoptotic rates of SiHa cells in the control group and experimental groups are 3.6% ± 1.5% (D1: Mock group), 18.9% ± 2.6% (D2: TCL–OXA–MDC1-AS group), and 29.9% ± 2.5% (D3: MTCL–OXA–MDC1-AS group).

Table 3 Effect of MDC1-as on SiHa Cell Proliferation (CCK-8 *a*-Value, $\bar{X} \pm S$)

Groups	24h	48h	72h
Mock	0.4230±0.0600	0.8162±0.1241	1.4505±0.1305
TCL-MDC1-AS	0.3905 ±0.0325*	0.6343±0.0920*	1.0148 ±0.1936*
MTCL-MDC1-AS	0.3704±0.0273*#	0.5589±0.1051*#	0.8559±0.1648*#

Notes: *P<0.05 compared with mock group; #P<0.05 compared with TCL–MDC1-AS group.

In vivo Tumor Inhibition Test

Through the tumor-bearing mice model, the in vivo antitumor activities of the different groups were evaluated. As shown in Figure 2C, on the 20th day after drug treatments, the tumor volumes of the control, OXA, TCL-OXA, TCL-MDC1-AS, TCL-OXA-MDC1-AS, and MTCL-OXA-MDC1-AS groups

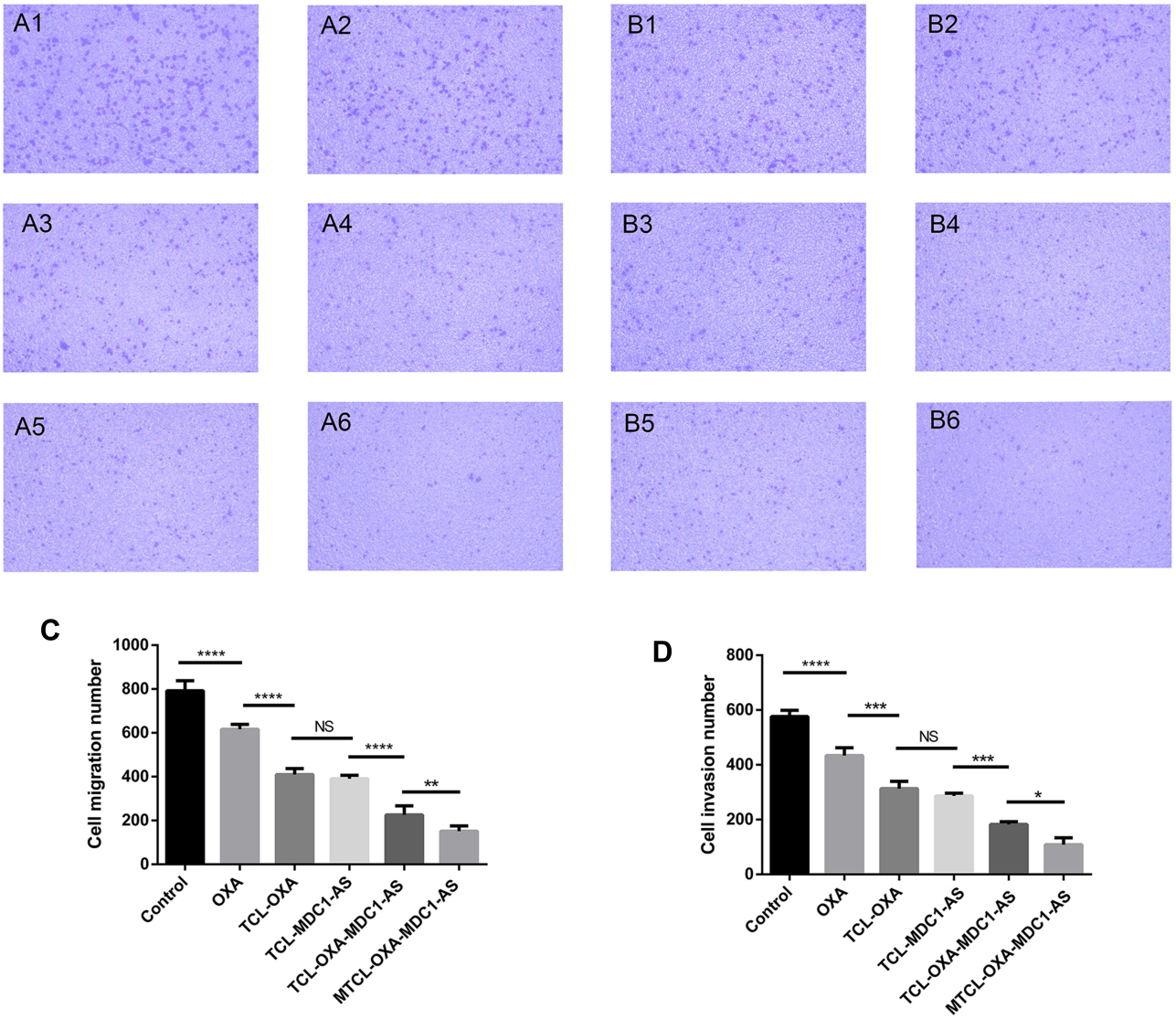

Figure 4 Cell migration and invasion assay of MTCL-OXA-MDC1-AS on SiHa cells. A, (**B**) The migration state (**A**) and invasion state (**B**) of SiHa cells in the control and experimental groups. Note: In the migration state of SiHa cells, A1-A6 respectively represent the control, OXA, TCL-OXA, TCL-MDC1-AS, TCL-OXA-MDC1-AS, and MTCL-OXA-MDC1-AS groups. In the invasion state of SiHa cells, B1-B6 respectively represent the control, OXA, TCL-OXA, TCL-MDC1-AS, TCL-OXA-MDC1-AS, and MTCL-OXA-MDC1-AS groups. C, (**D**) The migration number (**C**) and invasion number (**D**) of SiHa cells in the control and experimental groups. The values are expressed as mean ± SD (n=3). *P<0.05, **P<0.01, ***P< 0.001, ****P<0.0001.

were 3.56 ± 0.27, 2.57 ± 0.16, 1.78 ± 0.23, 1.86 ± 0.17, 1.04 ± 0.21, and 0.51 ± 0.3 cm^3, respectively. Moreover, as shown in Figure 2D, after combined therapy, the median survival time of the tumor-bearing mice was significantly extended. These results showed that the codelivery of OXA and MDC1-AS could generate synergistic antitumor effects. In vivo antitumor effect produced from the combined therapy was significantly stronger than that of a single application of OXA or MDC1-AS, and magnetic targeting could enhance the antitumor effect.

Expression of Apoptosis-Related Genes in Cervical Cancer

The RT-qPCR results showed that the expression levels of MDC1 and BAX in the tumor tissues in the MTCL-OXA-MDC1-AS group were the highest in all groups (ie, P<0.01, compared with the control group; P<0.01, compared with the OXA group; P<0.01, compared with the TCL-OXA group; P<0.01, compared with the TCL-MDC1-AS group; and P<0.05, compared with the TCL-OXA-MDC1-AS group) (Figure 5A and B). The RT-qPCR results showed that expression level of BCL-2 in the tumor tissues in the MTCL-OXA-MDC1-AS group was the lowest in all groups (ie, P<0.01, compared with the control group; P<0.01, compared with the OXA group; P<0.01, compared with the TCL-OXA group; P<0.01, compared with the TCL-MDC1-AS group; and P<0.05, compared with the TCL-OXA-MDC1-AS group) (Figure 5C).

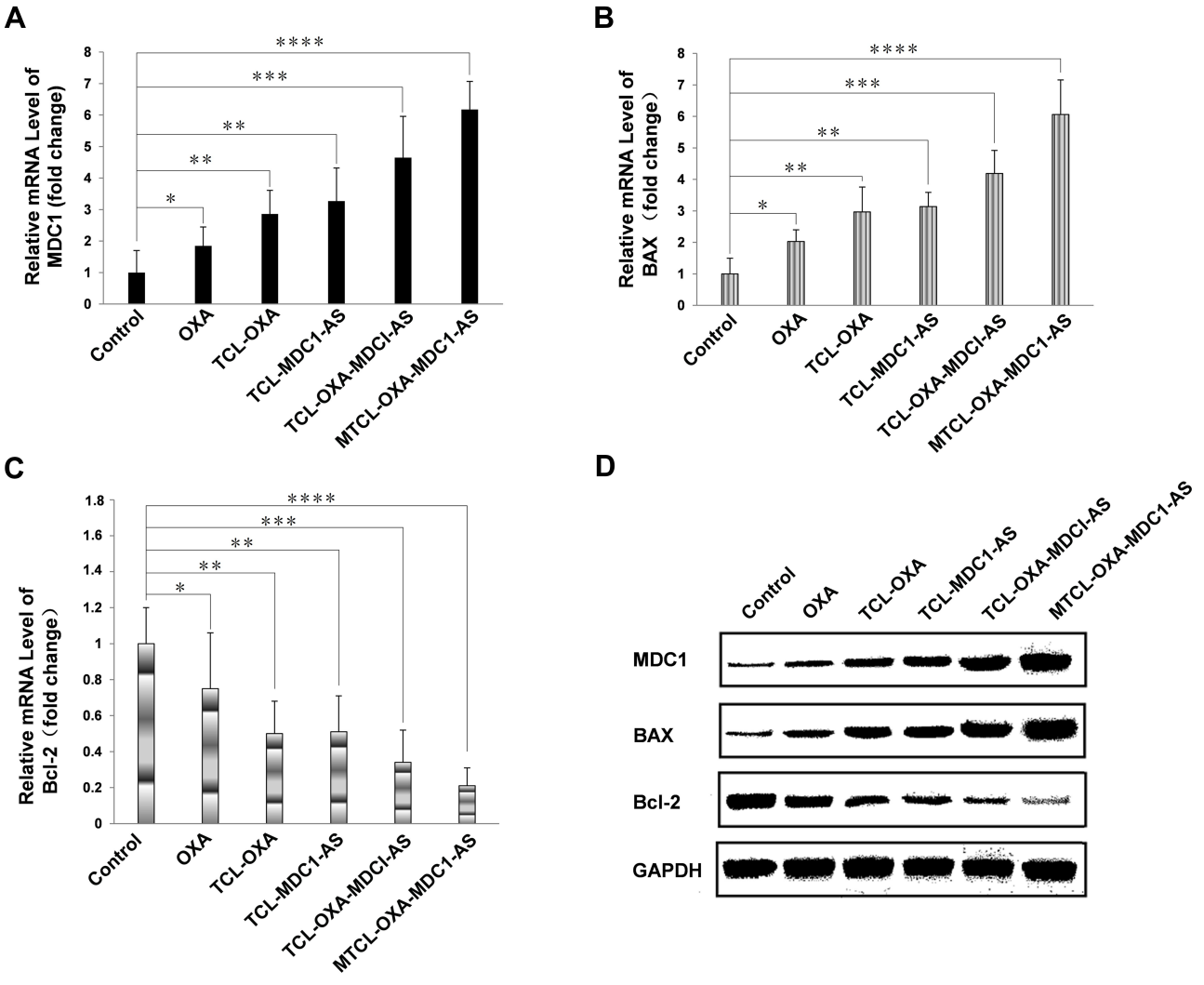

Figure 5 Expression of apoptosis-related genes in cervical cancer. (**A**–**C**) MDC1, BAX, and Bcl-2 expression in SiHa of each group as detected by RT-qPCR; (**D**) MDC1, BAX, and Bcl-2 expression in SiHa of each group as detected by Western blot analysis. The values are expressed as mean ± SD from three independent experiments. *P<0.05, **P<0.01, ***P<0.001, ****P<0.0001, significantly different from control group.

Western blot results showed that the expression levels of MDC1 and BAX in the tumor tissues in the MTCL-OXA-MDC1-AS group were the highest in all groups (ie, P<0.01, compared with the control group; P<0.01, compared with the OXA group; P<0.01, compared with the TCL-OXA group; P<0.01, compared with the TCL-MDC1-AS group; and P<0.05, compared with the TCL-OXA-MDC1-AS group) (Figure 5D). However, Western blot results showed that the expression level of BCL-2 in the tumor tissues in the MTCL-OXA-MDC1-AS group was the lowest in all groups (ie, P<0.01, compared with the control group; P<0.01, compared with the OXA group; P<0.01, compared with the TCL-OXA group; P<0.01, compared with the TCL-MDC1-AS group; and P<0.05, compared with the TCL-OXA-MDC1-AS group) (Figure 5D). The full blots for the Western blot of the apoptosis-related genes are shown in Figure S3.

Discussion

Cervical cancer is one of the most important diseases that affect women's health. The incidence of this cancer among young women has elevated significantly in recent years. Therefore, the disease has attracted increased concern and attention.[27] Chemotherapy has become an important approach for the treatment of Cervical cancer.[4] Nevertheless, this type of therapy cannot significantly change the prognosis of cancer patients.[7] One of the key reasons is that systemic drug distribution leads to limited drug concentration at the tumor site, generating numerous side effects. New drug delivery methods should be developed to solve the limitations of existing therapies. Targeted delivery systems enable drugs to reach the tumor site and control their release, thereby improving their therapeutic effects.[28–33] Another limitation of chemotherapy is the involvement of various oncogenes, antioncogenes, and drug resistance genes implicated in cancer occurrence and development. These oncogenes can invade, metastasize, and feature permanent biochemistry. In addition, drug resistance genes are directly mediated by multidrug resistance of cancer.[34] Therefore, multiagent codrug delivery system had been conceptualized. This system can codeliver two different drugs to the same tumor cell to perform a synergistic antitumor effect. This technique performs a synergistic antitumor effect with chemotherapy. The combined therapy has become a research hot spot.[28–30,32]

In multiple drug delivery systems, LPs show the greatest potential for development because of their superior biocompatibility (little to no antigen, allergy, and toxicity) and biodegradability. As a drug and gene carrier, LP can not only protect the host from the side effects of encapsulated drugs but also prevent premature inactivation of encapsulated drugs in the physiological medium.[35] Moreover, the LP can achieve passive targeting by improving the permeability and retention effect or achieve positive targeting through in vitro directed magnetic field guidance and immunization.[36] Various types of LP have been developed, and they do not interfere with the expression of certain genes in host cells.[37] For example, TL can release its contents at ambient temperature, with other features including optimal release timing and efficiency, thus enabling the local controlled release of drugs.[29,38] ML is enclosed by nano-ferro magnetic substances and can therefore move to the tumor site along the blood vessel under the guidance of in vitro directed magnetic field to achieve targeted delivery of loaded drugs.[7,26] The CL is a suitable gene carrier, which can carry an external gene into the cell to achieve gene transfection.[39] Numerous CLs have been applied to gene engineering.

In this study, the characteristics of TLs, MLs, and CLs were integrated to develop a novel MTCL. As shown in Figure 1, this novel LP consisted of thermosensitive phospholipid, nano-ferromagnetic substances, and cationic materials. Chemical drugs and magnetic nanoparticles were enclosed inside the LP. The gene vectors were placed on the surface through the electrostatic adsorption effect of cationic materials. The drug delivery system entered the body and moved to the local site of tumor under the effect of a permanent magnetic field to achieve magnetic targeting delivery. When the LP reached the tumor site, AMF on the ferroferric oxide core could function as the heat source. The phase transition of the thermosensitive phospholipids of the LP membrane occurred during thermotherapy. This phenomenon induced the release of chemical drugs in the drug carrier system to release and achieve in vitro thermosensitive controlled release. Agarose or native polyacrylamide electrophoresis have been approved to detect the stability of antisense lncRNA.[40,41] In future studies, this method could be considered to explore the influence of 42°C heat to the stability of antisense lncRNA. Meanwhile, the LP carrier nucleic acids can be used to treat oncogenes or drug-resistant genes. This technique forms a synergistic antitumor effect with chemotherapy. In this study, the LP thermosensitive formula in the literature was adapted;[42] that is, DPPC: DC-cholesterol:DOAB:cholesterol = 80:5:5:10. Satisfactory thermosensitive efficiency was obtained. Analysis using a vibrating sample magnetometer showed that MTCL

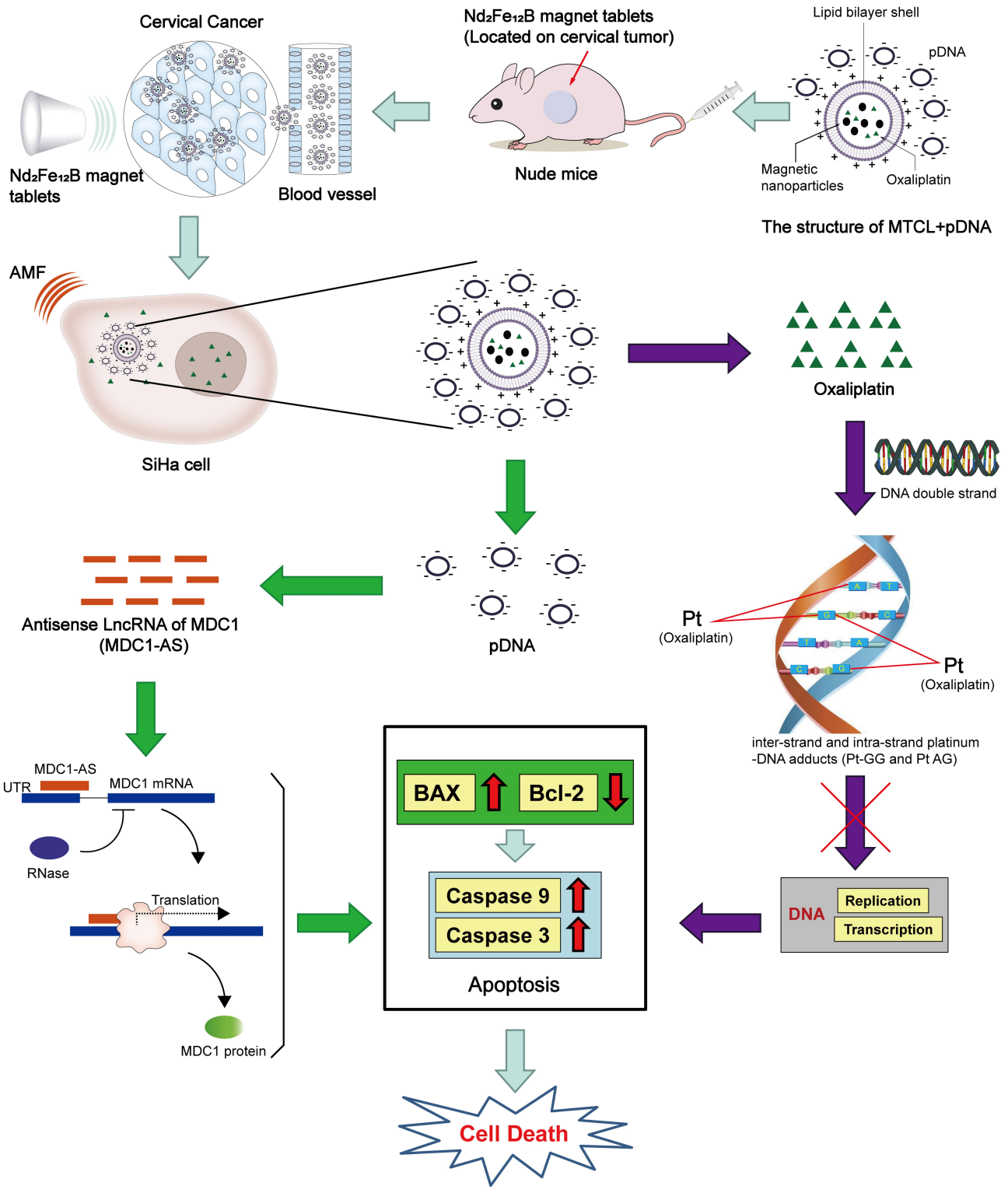

Figure 6 Sketch map of the structure and mechanism of the new magnetic thermosensitive cationic drug carrier system. The structural characteristics of MTCL drug carrier system include the nano Fe_3O_4 and OXA enclosed in a lipid bilayer, and the cationic lipid composition in the lipid bilayer is connected to the antisense lncRNA of MDC1. A large number of MTCLs can be accumulated in the tumor site under the magnetic traction at a certain intensity of an applied magnetic field to reduce the toxic and side effects on healthy cells and achieve the positive targeting of drugs. When the temperature in the tumor site increased from 37 °C to 42 °C under the effect of AMF in vitro, MTCL was triggered to release numerous drugs within a short time, thereby increasing drug content in the diseased site. In SiHa cells, MDC1-AS of MTCL can form RNA-RNA dimer with MDC1 and protect MDC1 from degradation by RNase, increasing the stability of MDC1 and elevating its expression level, while OXA of MTCL inhibited DNA replication and transcription by forming inter- and intra-strand platinum-DNA adducts. BAX increased and Bcl-2 decreased, activating caspase-3 and causing cell apoptosis in SiHa cells. The therapeutic effect was significantly improved through the synergistic mechanism.

exerted a good magnetic targeting effect. Meanwhile, the time–temperature dependence curve illustrated that, with the aid of a Fe_3O_4 magnetic fluid, the magnetic targeting of MTCL and controlled release of drug could be achieved. Finally, TEM results indicated that TCL and MTCL had typical morphology and satisfactory LP dispersion. From the successful construction of MTCL, OXA and the MDC1-AS plasmid was placed to MTCL to construct MTCL-OXA-MDC1-AS and evaluate the therapeutic effect for Cervical cancer in vivo and in vitro.

Under the effect of in vitro directed magnetic field, OXA and MDC1-AS carrier could be directed to the tumor site. However, the LP has low probability of being off targeted and accumulate in other organs. Performing fluorescent imaging after injection will be considered as a meaningful process in future studies.[41,43] Under the effect of AMF in vitro, OXA can be released thermosensitively. Thermosensitively released drugs depend on TL, which mainly consists of DPPC. DPPC can undergo phase transition from gel to liquid crystal state to release (leak) hydrophilic small molecular drugs at 41°C.[38] The results from differential scanning calorimetry showed that the T_m of the proposed delivery system was 40.8°C. In addition, analysis of the OXA release showed that the system was stable at 37°C. When the temperature was increased to 42°C, OXA was significantly released. Moreover, MDC1-AS loaded with thermosensitive CLs exerted no significant effect on the thermosensitive release of OXA. Therefore, the LP structure revealed satisfactory thermosensitivity and could be applied to thermosensitive controlled release of drugs in the local heating state.

As a type of drug carrier, magnetic targeting drugs (MDTs) can promote the accumulation of drugs in tumor target sites under in vitro directed magnetic field.[7,26,42,44] Meanwhile, gene delivery efficiency can be improved through the magnetic transfection of LPs by using MCLs.[45,46] In this study, MTCL-OXA-MDC1-AS was designed as a delivery system for the combination of MDT and magnetic transfection to promote the delivery efficiency of OXA and MDC1-AS. Compared with the mock and TCL-MDC1-AS groups, MTCL-MDC1-AS exhibited higher cytotoxicity for Cervical cancer cells, significantly enhanced apoptosis, and inhibited the migration and invasion activities of SiHa cells. Transplanted tumor test of nude mice with Cervical cancer in vivo showed that codelivery of OXA and MDC1-AS carrier presented strong inhibitory effect on the tumor growth under a magnetic field. In the SiHa cells, MDC1-AS of MTCL could form RNA-RNA dimer with MDC1 and thereby protect MDC1 from degradation by RNase. This process increased the stability and expression level of MDC1, while OXA of MTCL inhibited the replication and transcription of DNA by forming interstrand and intrastrand platinum-DNA adducts (Pt-GG and Pt-AG). Thus, BAX increased, and BCL-2 decreased. The eventual activation of caspase-3 caused cell apoptosis in the SiHa cells, resulting in the SiHa cell death, which significantly improved the therapeutic effect through the synergistic mechanism. In general, these data confirmed that the promotion of drug delivery efficiency and antitumor activity could be achieved under a magnetic field.

In summary, this study presents the principle of codelivery of OXA and MDC1-AS by a novel magnetic thermosensitive cationic drug carrier system for the treatment of Cervical cancer (Figure 6).

Conclusion

The novel codelivery system of drug and gene (MTCLs) possessed satisfactory combined characteristics of magnetic targeting under a directed magnetic field, thermosensitive controlled release triggered by AMF, and synergistic antitumor effect in vitro and in vivo. Therefore, the proposed codelivery system offers potential applications in the chemotherapy and gene therapy for Cervical cancer.

Abbreviations

AlphaMEM, a medium contains both essential and nonessential amino acids and can be used as a general purpose growth medium; AMF, alternating magnetic field; OXA, oxaliplatin; CL, cationic LPs; DPPC, 1,2-dipalmitoyl-sn-glycero-3-phosphocholine; DC-Chol, 3 ß-[N-(N', N'-dimethylaminoethane)-carbamoyl] cholesterol; DOAB, dimethyldioctadecyl ammonium bromide; LncRNA, long noncoding RNA; LP, liposomes; MDC1, the mediator of DNA damage checkpoint 1; MDC1-AS, antisense lncRNA of MDC1; MDR, multidrug resistance of cancer; ML, magnetic LP; MTCL-MDC1-AS, magnetic thermosensitive cationic liposome drug carrier, carrying the antisense lncRNA of MDC1; MTCL-OXA, magnetic thermosensitive cationic liposome drug carrier, carrying OXA; MTCL-OXA-MDC1-AS, MTCL as the carrier to co-deliver OXA and MDC1-AS; MTL, magnetic thermosensitive liposome; OXA, oxaliplatin; PBS, phosphate buffer saline; TCL-MDC1-AS, thermosensitive cationic liposome as the carrier to deliver MDC1-AS; TCL-OXA, thermosensitive cationic liposome as the carrier to deliver OXA; TCL-

OXA-MDC1-AS, thermosensitive cationic liposome as the carrier to co-deliver OXA and MDC1-AS; TEM, transmission electron microscopy; TL, thermosensitive LP.

Data Sharing Statement

All data included in this study are available upon request by contact with the corresponding author.

Ethics Approval

All animal experiments were approved and evaluated by the Animal and Ethics Review Committee of Wenzhou Medical University (Wenzhou Medical University Policy and Welfare Committee, Document ID: WMU-2011- AP-0013).

Consent for Publication

No human participants were involved with the study.

Acknowledgments

This work was supported by grants from the National Natural Science Foundation of China (82071836 to HY, 81371182, 81870810 to JL), Natural Science Foundation of Zhejiang Province, PRC (LY17H060008 to HY, LY14H140008 to ZC), Wenzhou Municipal Science and Technology Project for Public Welfare (Y2020240 to HY), Training Program of National College Students Entrepreneurship (201910343042X to ZW), Zhejiang College Students Innovative Entrepreneurial Training Program (2019R413025 to ZW).

Author Contributions

All authors made a significant contribution to the work reported, whether that is in the conception, study design, execution, acquisition of data, analysis and interpretation, or in all these areas; took part in drafting, revising or critically reviewing the article; gave final approval of the version to be published; have agreed on the journal to which the article has been submitted; and agree to be accountable for all aspects of the work.

Funding

This research did not receive any specific grant from funding agencies in the public commercial, or not-for-profit sectors.

Disclosure

The authors report no potential conflicts of interest for this work.

References

1. Chibwesha CJ, Stringer JSA. Cervical cancer as a global concern: contributions of the dual epidemics of HPV and HIV. *JAMA*. 2019;322(16):1558. doi:10.1001/jama.2019.16176
2. Hosseini ES, Meryet-Figuiere M, Sabzalipoor H, et al. Dysregulated expression of long noncoding RNAs in gynecologic cancers. *Mol Cancer*. 2017;16(1):1. doi:10.1186/s12943-017-0671-2
3. Costa SCSD, Bonadio RC, Gabrielli FCG, et al. Neoadjuvant chemotherapy with cisplatin and gemcitabine followed by chemoradiation versus chemoradiation for locally advanced cervical cancer: a randomized phase II trial. *J Clin Oncol*. 2019;37(33):3124–3131. doi:10.1200/JCO.19.00674
4. Xie Q, Liang J, Rao Q, et al. Aldehyde dehydrogenase 1 expression predicts chemoresistance and poor clinical outcomes in patients with locally advanced cervical cancer treated with neoadjuvant chemotherapy prior to radical hysterectomy. *Ann Surg Oncol*. 2016;1:163–170. doi:10.1245/s10434-015-4555-7
5. Ma J, Zeng S, Zhang Y, et al. BMP4 promotes oxaliplatin resistance by an induction of epithelial-mesenchymal transition via MEK1/ERK/ELK1 signaling in hepatocellular carcinoma. *Cancer Lett*. 2017;411.
6. Chen J, Jiang H, Wu Y, et al. A novel glycyrrhetinic acid-modified oxaliplatin liposome for liver-targeting and in vitro/vivo evaluation. *Drug Des Devel Ther*. 2015;9:2265–2275. doi:10.2147/DDDT.S81722
7. Ye H, Tong JS, Wu J, et al. Preclinical evaluation of rhIFN-α_2b-containing magnetoliposome for treating hepatocellular carcinoma. *Int J Nanomedicine*. 2014;9:4533–4550. doi:10.2147/IJN.S67228
8. Seyed Hosseini E, Alizadeh Zarei M, Babashah S, et al. Studies on combination of oxaliplatin and dendrosomal nanocurcumin on proliferation, apoptosis induction, and long non-coding RNA expression in ovarian cancer cells. *Cell Biol Toxicol*. 2019;35(3):247–266. doi:10.1007/s10565-018-09450-8
9. Shan K, Wang Y, Hua H, Qin S, Yang A, Shao J. Ginsenoside Rg3 Combined with oxaliplatin inhibits the proliferation and promotes apoptosis of hepatocellular carcinoma cells via downregulating PCNA and Cyclin D1. *Biol Pharm Bull*. 2019;42(6):900–905. doi:10.1248/bpb.b18-00852
10. Nagourney RA, Link JS, Blitzer JB, et al. Gemcitabine plus cisplatin repeating doublet therapy in previously treated, relapsed breast cancer patients. *J Clin Oncol*. 2000;18(11):2245–2249. doi:10.1200/JCO.2000.18.11.2245
11. Zhang P, Li J, Ghazwani M, et al. Effective co-delivery of doxorubicin and dasatinib using a PEG-Fmoc nanocarrier for combination cancer chemotherapy. *Biomaterials*. 2015;67:104–114. doi:10.1016/j.biomaterials.2015.07.027
12. Katayama S, Tomaru Y, Kasukawa T, et al. Antisense transcription in the mammalian transcriptome. *Science*. 2005;309:1564–1566.
13. Morris KV, Vogt PK. Long antisense non-coding RNAs and their role in transcription and oncogenesis. *Cell Cycle*. 2010;9(13):2544–2547. doi:10.4161/cc.9.13.12145
14. Xie S, Yu X, Li Y, et al. Upregulation of lncRNA ADAMTS9-AS2 promotes salivary adenoid cystic carcinoma metastasis via PI3K/Akt and MEK/Erk signaling. *Mol Ther*. 2018;26(12):2766–2778. doi:10.1016/j.ymthe.2018.08.018
15. Celano P, Berchtold CM, Kizer DL, et al. Characterization of an endogenous RNA transcript with homology to the antisense strand of the human c-myc gene. *J Biol Chem*. 1992;267:15092–15096. doi:10.1016/S0021-9258(18)42150-3
16. Faghihi MA, Modarresi F, Khalil AM, et al. Expression of a noncoding RNA is elevated in Alzheimer's disease and drives rapid feedforward regulation of beta-secretase. *Nat Med*. 2008;7:723–730. doi:10.1038/nm1784
17. Xue Y, Ma G, Zhang Z, et al. A novel antisense long noncoding RNA regulates the expression of MDC1 in bladder cancer. *Oncotarget*. 2015;6(1):1. doi:10.18632/oncotarget.2861

18. Yue H, Zhu J, Xie S, et al. MDC1-AS, an antisense long noncoding RNA, regulates cell proliferation of glioma. *Biomed Pharmacother*. 2016;81:203–209. doi:10.1016/j.biopha.2016.03.002
19. Bartkova J, Horejsi Z, Sehested M, et al. DNA damage response mediators MDC1 and 53BP1: constitutive activation and aberrant loss in breast and lung cancer, but not in testicular germ cell tumours. *Oncogene*. 2007;53:7414–7422. doi:10.1038/sj.onc.1210553
20. Motoyama N, Naka K. DNA damage tumor suppressor genes and genomic instability. *Curr Opin Genet Dev*. 2004;1:11–16. doi:10.1016/j.gde.2003.12.003
21. Teo P, Cheng W, Hedrick JL, Yang YY. Co-delivery of drugs and plasmid DNA for cancer therapy. *Adv Drug Deliv Rev*. 2016;98:41–63. doi:10.1016/j.addr.2015.10.014
22. Ta T, Porter TM. Thermosensitive liposomes for localized delivery and triggered release of chemotherapy. *J Controlled Release*. 2013;169(1–2):112–125. doi:10.1016/j.jconrel.2013.03.036
23. Haemmerich D, Motamarry A. Thermosensitive liposomes for image-guided drug delivery. *Adv Cancer Res*. 2018;139:121–146.
24. Uppu DS, Haldar J. Lipopolysaccharide neutralization by cationic-amphiphilic polymers through pseudoaggregate formation. *Biomacromolecules*. 2016;17(3):862–873. doi:10.1021/acs.biomac.5b01567
25. Zhu KY, Palli SR. Mechanisms, applications, and challenges of insect RNA interference. *Annu Rev Entomol*. 2019;65:1.
26. Hui Y, Tong J, Liu J, et al. Combination of gemcitabine-containing magnetoliposome and oxaliplatin-containing magnetoliposome in breast cancer treatment: a possible mechanism with potential for clinical application. *Oncotarget*. 2016;28:43762–43778.
27. R S S, Jain A, Zhao Z, et al. Intracellular trafficking and exocytosis of a multi-component siRNA nanocomplex. *Nanomedicine*. 2016;12(5):1323–1334. doi:10.1016/j.nano.2016.02.003
28. Xiao Y, Jaskula-Sztul R, Javadi A, et al. Co-delivery of doxorubicin and siRNA using octreotide-conjugated gold nanorods for targeted neuroendocrine cancer therapy. *Nanoscale*. 2012;4(22):7185–7193. doi:10.1039/c2nr31853a
29. Shim G, Han SE, Yu YH, et al. Trilysinoyl oleylamidebased cationic liposomes for systemic co-delivery of siRNA and an anticancer drug. *J Control Release*. 2011;155:60–66. doi:10.1016/j.jconrel.2010.10.017
30. Shen J, Yin Q, Chen L, et al. Co-delivery of paclitaxel and survivin shRNA by pluronic P85-PEI/TPGS complex nanoparticles to overcome drug resistance in lung cancer. *Biomaterials*. 2012;33(33):8613–8624. doi:10.1016/j.biomaterials.2012.08.007
31. Chen Y, Bathula SR, Li J, et al. Multifunctional nanoparticles delivering small interfering RNA and doxorubicin overcome drug resistance in cancer. *J Biol Chem*. 2010;285(29):22639–22650. doi:10.1074/jbc.M110.125906
32. Liu C, Liu F, Feng L, et al. The targeted co-delivery of DNA and doxorubicin to tumor cells via multifunctional PEI-PEG based nanoparticles. *Biomaterials*. 2013;34(10):2547–2564. doi:10.1016/j.biomaterials.2012.12.038
33. Zhao F, Yin H, Li J. Supramolecular self-assembly forming a multifunctional synergistic system for targeted co-delivery of gene and drug. *Biomaterials*. 2014;35(3):1050–1062. doi:10.1016/j.biomaterials.2013.10.044
34. Szakacs G, Paterson JK, Ludwig JA, et al. Targeting multidrug resistance in cancer. *Nat Rev Drug Discov*. 2006;3:219–234.
35. Juergen S, Ronald AS, Michael JR. *Fundamentals and Applications of Controlled Release Drug Delivery*. Springer-Verlag New York Inc press; 2012:291.
36. Torchilin VP. Passive and active drug targeting: drug delivery to tumors as an example. *Handb Exp Pharmacol*. 2010;197:3–53.
37. He K, Tang M. Safety of novel liposomal drugs for cancer treatment: advances and prospects. *Chem Biol Interact*. 2018;295:13–19. doi:10.1016/j.cbi.2017.09.006
38. Fei Y, Wanlu D, Yekuo L, et al. NIR-laser-controlled drug release from DOX/IR-780-loaded temperature-sensitive-liposomes for chemo-photothermal synergistic tumor therapy. *Theranostics*. 2016;6(13):2337–2351. doi:10.7150/thno.14937
39. Ren J, Yu C, Wu S, et al. Cationic liposome mediated delivery of FUSl and hIL-12 coexpression plasmid demonstrates enhanced activity against human lung cancer. *Curr Cancer Drug Targets*. 2014;2(2):167–180. doi:10.2174/1568009614666140113115651
40. Jain A, Barve A, Zhao Z, et al. Comparison of avidin, neutravidin, and streptavidin as nanocarriers for efficient siRNA delivery. *Mol Pharm*. 2016;14:5.
41. Zhao Z, Li Y, Jain A, et al. Development of a peptide-modified siRNA nanocomplex for hepatic stellate cells. *Nanomedicine*. 2017;14:1. doi:10.1016/j.nano.2017.08.017
42. Pradhan P, Giri J, Rieken F, et al. Targeted temperature sensitive magnetic liposomes for thermo-chemotherapy. *J Control Release*. 2010;142(1):108–121. doi:10.1016/j.jconrel.2009.10.002
43. M J D, C Q W, G L W, et al. Development of novel long noncoding RNA MALAT1 near-infrared optical probes for in vivo tumour imaging. *Oncotarget*. 2017;8(49):85804–85815. doi:10.18632/oncotarget.20652
44. Alexiou C, Arnold W, Klein RJ, et al. Locoregional cancer treatment with magnetic drug targeting. *Cancer Res*. 2000;60:6641–6648.
45. Zheng X, Lu J, Deng L, et al. Preparation and characterization of magnetic cationic liposome in gene delivery. *Int J Pharm*. 2009;366(1–2):211–217. doi:10.1016/j.ijpharm.2008.09.019
46. Wang C, Ding C, Kong M, et al. Tumor-targeting magnetic lipoplex delivery of short hairpin RNA suppresses IGF-1R overexpression of lung adenocarcinoma A549 cells in vitro and in vivo. *Biochem Biophys Res Commun*. 2011;410(3):537–542. doi:10.1016/j.bbrc.2011.06.019